RGNZ/MGPB

Deep Ground Penetrating Radar Imaging for the purpose of exploring ore and geological structures in the Calamine Mine, Central Iran

Rudarsko-geološko-naftni zbornik
(The Mining-Geology-Petroleum Engineering Bulletin)
UDC: 622.1 > 550.8
DOI: 10.17794/rgn.2024.5.1

Original scientific paper

Nasrin Sadrmohammadi[1]; Selma Kadioğlu[2]; Khalil Rezaei[3]; Mahmoud Honarvar[4]

[1] *Department of Geology, Kharazmi University, Iran. 0000-0002-7193-2222*
[2] *Department of Geophysical Engineering, Ankara University, Turkey. 0000-0002-5839-3957*
[3] *Department of Geology, Kharazmi University, Iran. 0000-0001-7997-7196*
[4] *Zap consulting engineers, Iran.*

Abstract

This study aimed to identify mineralized zones within a sedimentary structure, including its discontinuities such as layer boundaries, and faults. The Loza-N model Deep Ground Penetrating Radar (DGPR) system with a 25 MHz antenna was employed to achieve a target depth of up to 200 meters. The investigation was conducted on mine terraces, berms, and the flat northern part of the Mehdiabad calamine mine located in Yazd, Iran. A total of 23 profiles were surveyed. Data acquisition for some profiles involved parallel transects, while others utilized a series approach where the transmitter and receiver antennas were progressively moved along the ground surface. The processed radargrams from selected profiles were compared amongst themselves and with borehole data collected along the same profiles. The geological structure was successfully visualized using two different software programs. Krot software effectively distinguished all limestone units and their zonation. By combining the GPR data with borehole results, it was possible to identify potential ore mineral zones within the marly units. Based on the DGPR traces at borehole locations, high-grade ore minerals in the marly limestone exhibited positive phase and amplitude values, represented by intermediate to maximum color hues. Conversely, light green and light gray limestone containing iron oxide and calcite veins displayed negative phase and amplitude values, with negative zero to intermediate color hues. Dark green limestone showed the most negative phase and amplitude values, reflected by the maximum negative color hues. Finally, light red limestone, likely containing low-grade ore, presented positive but minimal phase and amplitude values, visualized by positive minimum color hues.

Keywords:
Deep Ground Penetrating Radar (DGPR); Loza-N DGPR System; geological structure; limestone units; Mehdiabad calamine mine

1. Introduction

Ground Penetrating Radar (GPR) has emerged as a prominent geophysical method due to its wide range of applications, stemming from its exceptional strengths. High Resolution: GPR offers high-resolution imaging of subsurface structures, allowing for the detailed analysis of underground features. Rapid Data Acquisition: GPR surveys can be conducted efficiently, enabling rapid data collection and project completion. Cost-Effectiveness: compared to alternative geophysical methods, GPR is relatively inexpensive, making it an attractive option for various applications. Low Environmental Noise Interference: GPR is minimally affected by ambient noise, ensuring reliable data acquisition even in challenging environments. Non-Destructive Methodology: GPR is a non-invasive technique, causing no damage to the surveyed materials or structures. These attributes have made GPR a valuable tool for a diverse array of scientific investigations, including: the detection of subsurface cavities (**Kofman et al., 2006; Kadioglu and Ulugergerli, 2012**), the detection of faults (**He et al., 2013; Zhao et al., 2015; Akyüz et al., 2019; Stemberk et al., 2019; Liang et al., 2019; Wong et al., 2019**), the investigation of qualitative and quantitative properties of faults, such as the detection of the exact direction, dip angle of faults and also hidden faults (**Lunina et al. 2018; Nakanishi et al., 2017; Brandes et al., 2018; Rezaei et al., 2019; Aliyannezhadi et al., 2020**), fractures (**Elkarmoty et al., 2017**), sedimentology (**Gu et al., 2018**), landslide (**Rehman et al., 2021**), archeology, military and civil engineering (**Daniels, 1989; Davis and Annan, 1989; Kadioglu and Daniels, 2008; Kadioglu et al., 2013a, 2013b; Kadioglu and Kadioglu, 2016; Kadioglu, 2018**).

Generally, the effectiveness of GPR hinges on four key factors: transmitting frequency, antenna design, the electrical properties of the target area (ground or material), and the electrical contrast between the targets and

Corresponding author: Nasrin Sadrmohammadi
e-mail address: nasrin_sadrmohammady@yahoo.com

their surroundings. There's a trade-off: higher frequencies provide finer resolution but limited penetration depth, while lower frequencies penetrate deeper but offer poorer resolution.

Driven by the burgeoning global economy, the expansion of the industrial sector in many nations, and the escalating international demand for mineral resources, mining has garnered significant attention. Novel exploration techniques and the utilization of metals in cutting-edge technologies have reshaped the nature of societal demand for mineral resources. Traditionally, GPR has been employed in near-surface mining investigations due to its cost-effectiveness in preliminary studies, encompassing: GPR mapping of the structural properties of Quaternary sediments in Siilinjärvi mine (**Luoma et al., 2016**), exploration and evaluation of the GPR method in relation to mineralization zones (**Patterson and Cook, 2002; Singh and Chauhan, 2002; Francke and Utsi, 2009; Francke, 2010; Manu et al., 2013; Ralston and Strange, 2015, Berkut et al., 2017; Zanzi et al., 2017**), assessment of the potential risks and catastrophes in coal mines (**Xu et al., 2018**), the study and identification of karst cavities in mines (**Baggett et al., 2019**). However, GPR's effective depth was limited (30-40 meters in rock, 10-15 meters in soil), posing a challenge for geologists (**Kopeikin et al., 2012**) and miners who require deeper exploration. Deep GPR (DGPR) technology has emerged to address this limitation, and the Loza series devices are particularly well-suited for such deep-exploration applications in geological and mining studies. Loza series instruments stand out for their ability to operate in highly conductive environments, such as loam or wet clay. This is achieved through several key features:

- High-energy pulses: a high-voltage gas discharge tube (peak voltage of 5-10 kV) generates powerful radar pulses.
- Resistively loaded dipole antenna: the antenna design (0.5 to 6 meters long) efficiently transmits these pulses.
- Low-frequency emphasis: signal energy concentrates in the lower frequencies, improving penetration in conductive materials.
- Large dynamic range: the instruments can capture a wide range of echo signal strengths, allowing the detection of faint signals from deep targets.

Combined, these features empower Loza devices to study previously inaccessible subsurface structures in challenging environments (**Kopeikin et al., 1996, 2013; Popov et al., 2017; Prokopovich et al., 2018b**). In the following section, various applications of Loza devices in scientific research are described. In August 2017, Di Marzo and colleagues employed the latest generation of Loza-2N ultra-deep GPR technology to conduct a comprehensive subsurface investigation in the "il Lago" region. The system's exceptional capabilities enabled them to successfully penetrate depths of up to 400 meters, revealing the detailed geological stratigraphy and identifying both horizontal and vertical discontinuities in the underlying strata. These findings were based on a thorough analysis of the characteristics of reflected waves, including their density, amplitude, continuity, and diffraction geometry. The study also revealed the presence of buried faults within the subsurface. The results of this groundbreaking research were published in the following year (**Di Marzo et al., 2018**). Kopeikin and his colleagues demonstrated the effectiveness of Loza-N and Loza-V series devices in accurately identifying the optimal drilling locations for oil and gas pipelines (**Kopeikin et al., 2012**). Leveraging the capabilities of Loza-N GPR technology, Kopeikin and his team meticulously scanned the depths of Lake Chebarkul at the site of the Chelabinsk Meteorite impact, successfully uncovering the remnants of the meteorite (**Kopeikin et al., 2013**). Morozov and his colleagues used Loza-N and Loza-V devices in order to investigate the archaeological and geographical situation of the ancient region (**Morozov et al., 2023**). The scientific research conducted by Prokopovich and his colleagues using the Loza-N device aimed to investigate buried riverbeds or the interface between natural and artificial lands in the Black Sea coastal area near Odessa. The research has provided good results (**Prokopovich et al., 2018b**). Pupatenko and his colleagues used the Loza-N device in 2017 and 2019 to investigate the slope of subsurface layers and to prevent potential road construction problems and deformation of the railway substructure (**Pupatenko et al., 2017, 2019**).

The sedimentary deposits of the Mehdiabad mine complex in Yazd are of great importance due to their high content of lead-zinc and barium elements. Over the years, numerous scientific research projects have been conducted in this mining complex, which are described below. In his Ph.D. thesis, Reichert proposed a metallogenetic model for carbonate hosted non-sulfide zinc deposits based on the observations of Mehdiabad and Iran Kouh, Central and Southwestern Iran (**Reichert, 2007**). The M.Sc. theses by Ghasemi, Ebrahim Mohseni, and Pourfaraj respectively investigated the geochemistry and mineralization style of the Mehdiabad mine complex, the fluid inclusion and the determination of the ore genesis, and the faults of the complex. Maghfouri, in his PhD dissertation, comprehensively studied the geological setting, geochemistry, ore controlling parameters and genesis of Early Cretaceous carbonate-clastic hosted Zn-Pb deposits in Southern Yazd basin, with an emphasis on the Mehdiabad deposit in the Mehdiabad complex (**Ghasemi, 2006; Ebrahim Mohseni, 2011; Pourfaraj, 2016; Maghfouri, 2017**). In 2018, Hashemi Marand and his colleagues conducted scientific research to determine the relationship between silver and lead mineralization based on fractal modelling in the Mehdiabad deposit in Central Iran (**Hashemi Marand et al., 2018**).

With the resumption of mining activities at the calamine mine in the Mehdiabad mining complex, there was

a need to obtain integrated subsurface information from great depths of the mine in the shortest possible time for the selection of drilling areas and analysis of core samples. In order to investigate the potential mineralization zones and faults in the limestone rocks of the calamine mine, we used the Loza-N device with a 25 MHz antenna and a penetration depth of 200 meters. This was done after gaining information about the application of new Loza devices with a very high penetration depth. A new Loza-N DGPR system equipped with transmitter antennas was used, which exceeded 10-100 times the maximum transmitter power of conventional GPRs. It was also equipped with a low-frequency resistive load antenna (**Kopeikin et al., 2013; Buzin et al., 2017; Prokopovich et al., 2018a; Pupatenko et al., 2019**). Thus, the main problem of penetration depth in the design of this device compared to other older GPR devices has been solved and can be evaluated and validated by the results of this research. This research also demonstrates the valuable application of the Loza-N device in this mining sector, which is being presented for the first time in Iran. Furthermore, based on the presented results, it can be applied to other mining regions. The following section will discuss the geographical location and geology of the calamine mine, as well as provide an explanation of the Loza DGPR device and the data acquisition and processing methods.

2. Methodology

Subsequent to field visits and geological surveys (Preparation of Thin-sections and polished sections) conducted at the Mehdiabad Mining Complex, the calamine mine was meticulously examined as the study area for this paper. GPR survey lines were meticulously designed based on geological maps, surface outcrops of geological formations, and alteration studies within the study area. GPR survey lines totaling 3505 meters were implemented using 25 MHz antenna and 3505 meters were implemented using 50 MHz antenna along accessible routes, terraces, and berms (a total of 23 profiles). The results presented in this paper are based on data from the 25 MHz antenna. Due to the large number of profiles, only a few of them were analyzed. Using the results of DGPR, 53 boreholes were drilled in the calamine mine. This paper provides a detailed description of the geology, specifications of the DGPR system used, and data acquisition and processing methods.

2.1. Geographical setting

The Mehdiabad mining complex is located in the Yazd Block (**Stöcklin, 1968**) (see **Figure 1A, B**). It lies 110 kilometers southeast of Yazd city and 18 kilometers northeast of Mehdiabad village. The complex encompasses three mining sectors: Lead-Zinc, Barite (see **Figures 1C** and **2**), and Calamine (see **Figure 1C, D**). The Mehdiabad calamine mine, the area of study, covers 54 hectares and is situated north of the Lead-Zinc and Barite mines (see **Figure 2**).

2.2. Geology

Mineral resources and mineralization in the Mehdiabad mining complex are widespread within Lower Cretaceous carbonate rocks, including the Sangestan, Taft, and Abkuh formations. The Sangestan Formation, the oldest in the area, is located at the mine's lower altitude. It is comprised of siltstone, shaly limestone, sandy limestone, and bioclastic limestone interbedded with sandstone. The Taft Formation overlies the Sangestan Formation in this area. The Taft Formation consists mainly of carbonate and dolomite rocks, with karst features evident in the upper horizons. Mineralization is hosted within the dolomite section. The Abkuh Formation is the youngest formation studied here. It comprises limestone units, along with clayey and cherty limestones. Lead and zinc mineralization (carbonate and silicate minerals) is present in the lower part of this formation (**BRGM, 1994**). Notably, the Abkuh Formation, dating back to the Cretaceous (Albian) period, also serves as the host rock for the calamine mine. This mine contains the oldest mineral extracted in the Mehdiabad mining complex and central Iran. Within the study area, the Abkuh Formation can be further divided into four separate units: K_a^{sh1}, K_a^{l2}, K_a^{l3}, and K_a^{l4} (see **Figure 3**).

Faults with normal and strike-slip mechanisms are considered the primary cause of mineralization in the region (**Pourfaraj, 2016**). A mineralogical study of the ores reveals sphalerite and galena as the major sulfide minerals, with barite, pyrite, and chalcopyrite as minor constituents. The oxide ores, on the other hand, are dominated by cerussite ($PbCO_3$), smithsonite ($ZnCO_3$), hemimorphite ($Zn_4(Si_2O_7)(OH)_2 \cdot H_2O$), and hydrozincite ($Zn_5(CO_3)_2(OH)_6$). The mineral assemblage in this ore deposit typically exhibits layered, lenticular, and isoclinal morphologies, often conforming to the layering of the host rocks. Visible concentrations of minerals are also observed within cracks and karst cavities (**BRGM, 1994; Reichert et al., 2003; Borg, 2005; Reichert, 2007; Maghfouri, 2017; Maghfouri et al., 2019; Sadrmohammadi et al., 2021**). The barite mine (see **Figure 2**), located in the lower part of the Abkuh Formation and situated near the main pit of the lead-zinc mine, has garnered economic interest due to its barite ore deposit.

The Mehdiabad calamine mine is situated northwest of the Mehdiabad mining complex's main pit (see **Figure 1C, D**). This section of the mine exclusively contains non-sulfide lead-zinc deposits, separated from other areas by faults. The rock matrix of this carbonate formation is thought to have formed due to fault activity and brecciation of karst features in the area. The Black Hill fault (right-reverse mechanism) and the northern Forouzandeh fault (right-normal mechanism) are the most significant faults within the mine. Both faults dip towards the northeast. Based on mineral grades obtained

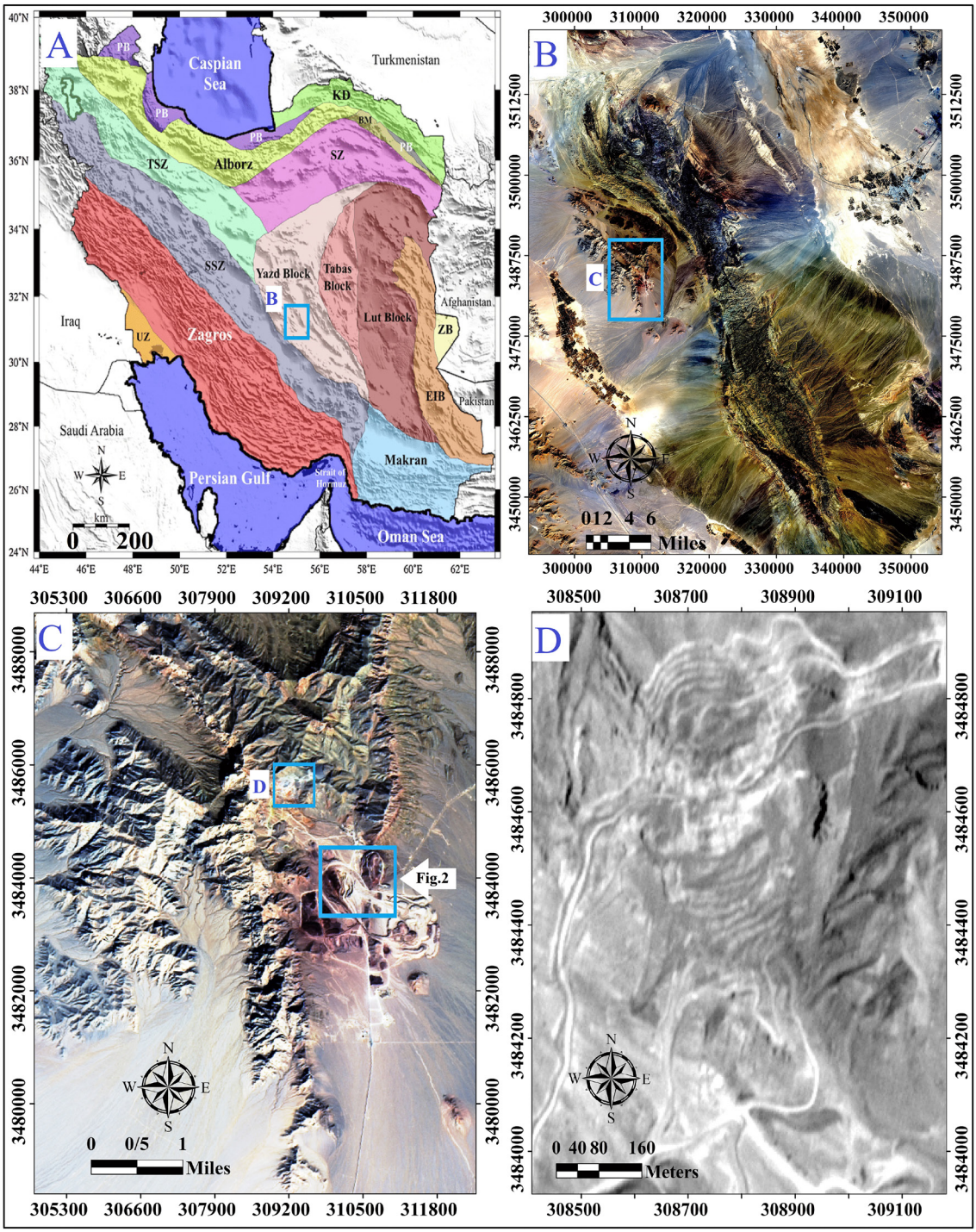

Figure 1: (A) Geological zones of Iran, (B) Location of the Mehdiabad mining complex within the southern block of Yazd, (C) Distribution of lead-zinc, barite mines, and the Mehdiabad calamine mine, (D) Satellite image (source: IRS) of the Mehdiabad calamine mine.

from drilling boreholes analyzed in this paper, the calamine mine's deposits can be broadly categorized into three distinct lenses at varying elevations: 2006 meters, 2080 meters, and 2230 meters, respectively (see **Figures 4** and **5**). In addition to these three main lenses, smaller to medium-sized veins outcrop in the area. As indicated in the 1:1000 scale geological map (see **Figure 3**), the calamine lenses and veins are positioned within the central reefal-karstic unit and are classified as Zn-Pb ore. The studied area exhibits mineralization with zinc and lead minerals. In the oxidized zone, zinc is present as hydrozincite, hemimorphite, and smithsonite, while lead occurs as cerussite and anglesite. In some areas, the calamine deposit also contains sulfide minerals of zinc (sphalerite) and lead (galena), along with iron and manganese oxides/hydroxides. Additionally, zincite and goe-

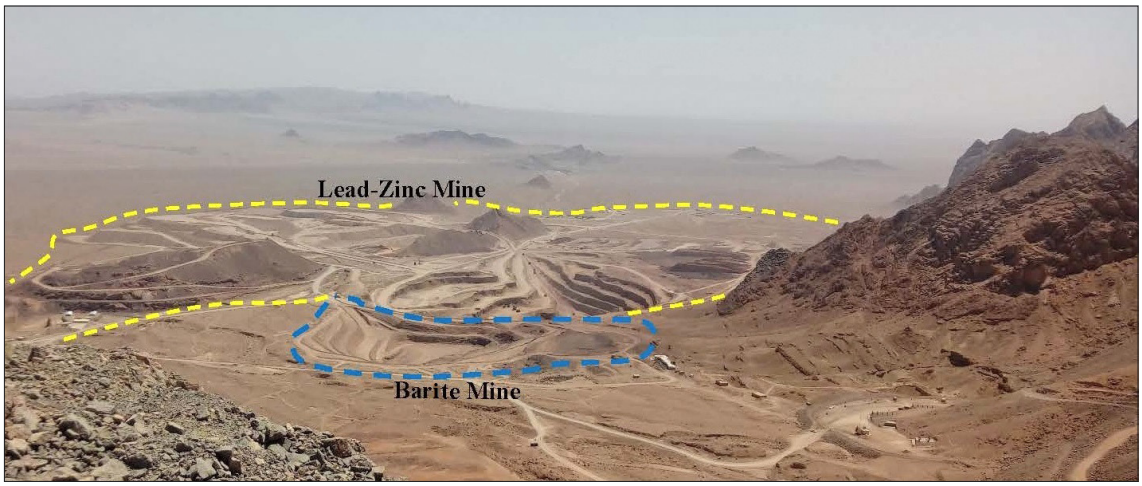

Figure 2: View of the main lead-zinc and barite mine pits (looking south)

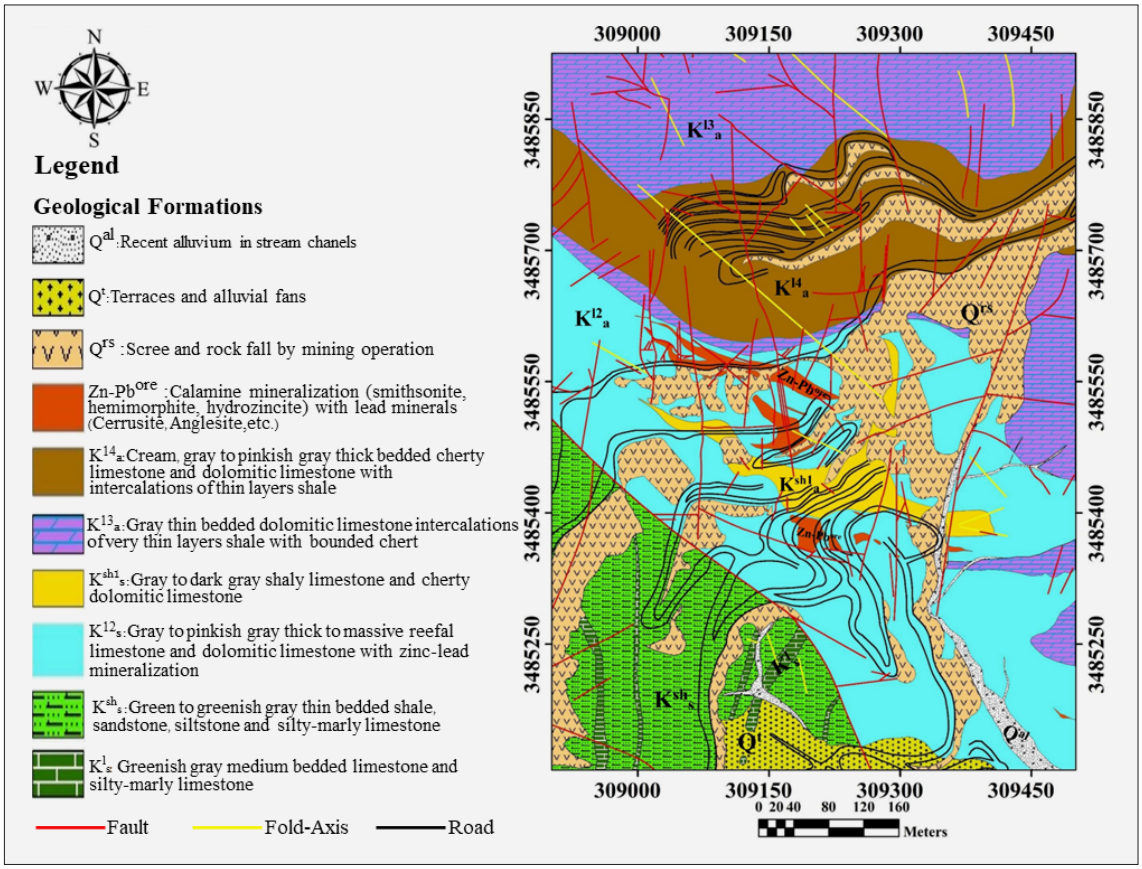

Figure 3: Geological map of the Mehdiabad calamine mine (scale 1:1000) (prepared by **Kousha Mine Company, 2017**)

thite have been identified in localized zones (see **Figure 6**). Minor occurrences of other minerals such as mimetite, hetaerolite, and sauconite are also reported.

2.3 Deep Ground Penetrating Radar (DGPR)

Traditional Ground Penetrating Radar (GPR) methods are typically limited to investigating shallow ore deposits, reaching depths of approximately 20-30 meters under ideal conditions (low weathering and sedimentary clay range). However, the study area at the Mehdiabad calamine mine presented challenges: significant weathering in the shallow subsurface with a carbonate host rock (as shown in **Figure 4**) and a highly variable and complex carbonate structure. While a traditional 25 MHz antenna GPR system might have achieved a depth of 30-40 meters, imaging beyond 40 meters was necessary.

Deep Ground Penetrating Radar (DGPR) systems offered a potential solution for reaching depths of 150-200 meters. However, their effectiveness in overcoming the

Figure 4: Views of excavation and sampling activities related to exploration boreholes identified using DGPR results at the Yazd calamine mine.

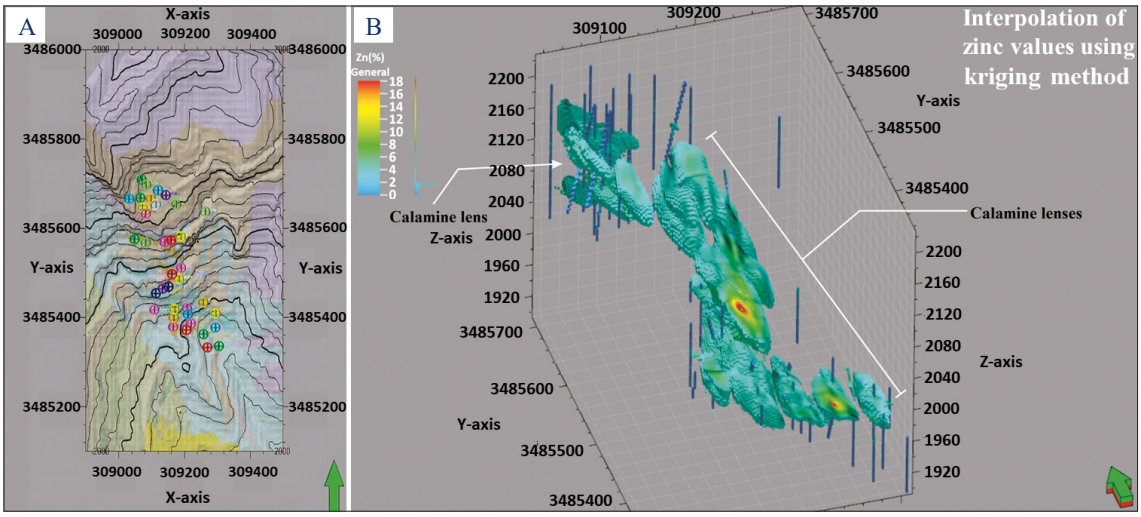

Figure 5: (A) Location of DGPR exploration boreholes on the topographic map of the calamine mine, (B) Visualization of the calamine ore deposit shape obtained by kriging interpolation of analyzed zinc element data from core samples.

specific challenges of this area was unknown. This study aimed to evaluate the applicability of DGPR for investigating deeper targets and assess the capabilities of a new generation GPR system, the Loza-N system. The Loza-N system boasts several key technical features (**Prokopovich et al., 2018b**):

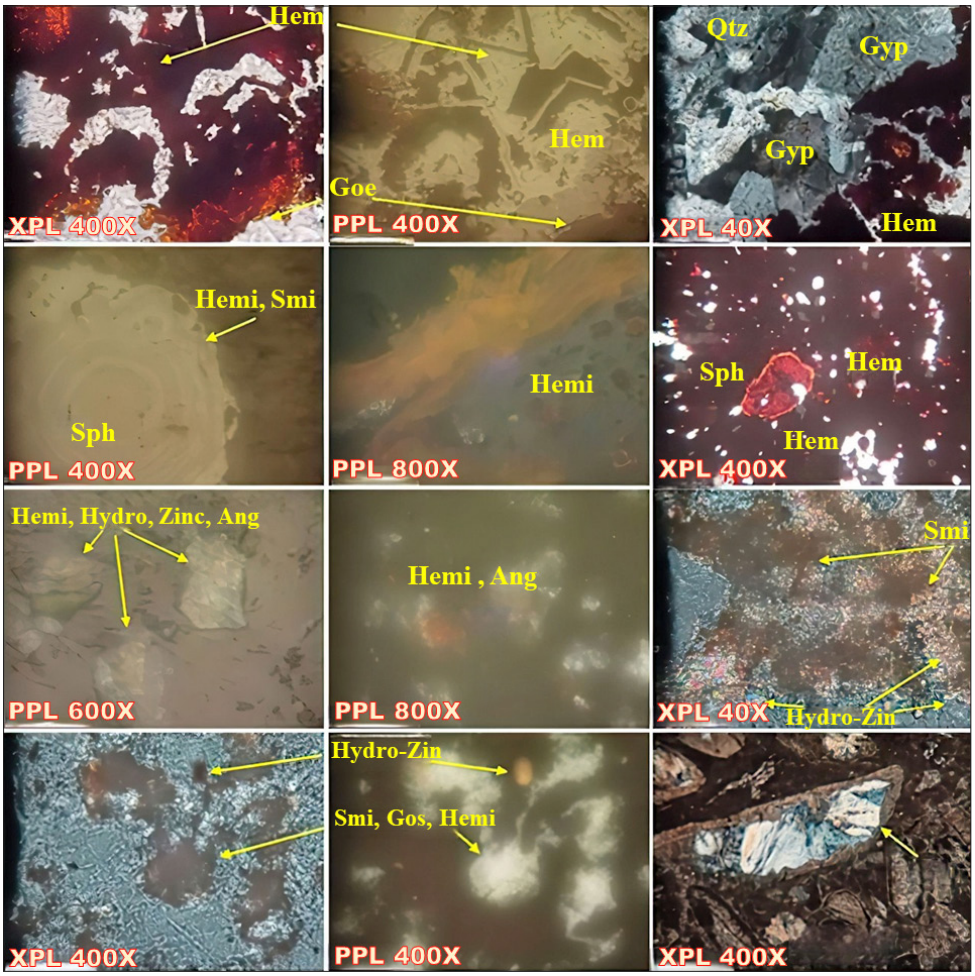

Figure 6: Microscopic Observations; Goethite Replacement: replacement of the goethite's "tooth-texture" resulted in a pseudo-growth pattern of fine hematite observed under both transmitted and polarized light (XPL/PPL 400X). Zinc Mineral Intergrowths: intergrowths of various zinc minerals were observed, including smithsonite, hemimorphite, sulfides, silicates, and hydrozincite with a colloidal texture (PPL 400X, 600X; XPL 40X, 400X). Iron Oxide Effects: the presence of goethite mineralization and iron oxides is evident. Anglesite and hemimorphite minerals were identified. Smithsonite appeared colorless or faintly colored under transmitted light, while hydrozincite was also observed. Goethite and anglesite minerals were identified using XPL 800X and PPL 400X magnification. Sphalerite Replacement: replacement of zinc, iron, and manganese around the sphalerite mineral was observed under XPL 100X magnification. Sphalerite Texture: sphalerite exhibited a concentric "chloroform texture," with color variations across different zones likely due to changes in iron content (PPL 400X).

- Receiver frequency band: 1-50 MHz.
- Antennas: Resistively loaded half-wavelength dipoles of Wu-King type with central frequencies ranging from 25 MHz (6 meters) to 50 MHz (3 meters).
- Transmitter voltage: 10 and 21 kV.
- Pulse repetition rate: 150-200 s^{-1}.
- Radar potential (maximum transmitted over minimum received signal): At least 120 dB (**Popov et al., 2017**).

The Georadar Loza-N utilizes serial transmitters with voltages of 5, 10, 15, and 21 kV. The weakest transmitter offers an estimated power of 1 MB per pulse. These transmitters function under diverse weather conditions and, due to their short pulse duration, do not interfere with radio or television broadcasts. In specific situations, higher voltage transmitters can be employed.

2.3.1. DGPR Data Acquisition

This study employed a Loza-N model GPR system, a new generation device designed by the Pushkov Institute of Terrestrial Magnetism, Ionosphere, and Radio Wave Propagation of the Russian Academy of Sciences (IZMIRAN) and VNIISMI Company (**Kopeikin et al., 1996; URL1, 1996**). The Loza-N system boasts peak power exceeding traditional GPR systems by 10,000 to 100,000 times (**Kopeikin et al., 2013; Buzin et al., 2017**). According to specifications, it can achieve a maximum investigation depth of 200 meters using a resistively loaded dipole antenna and a peak voltage of 21 kV at 15-20 MHz (**Buzin et al., 2017**).

A 25 MHz Loza-N system antenna with a length of 6 meters was used to acquire data across 23 profiles within the study area. Data acquisition employed a combination

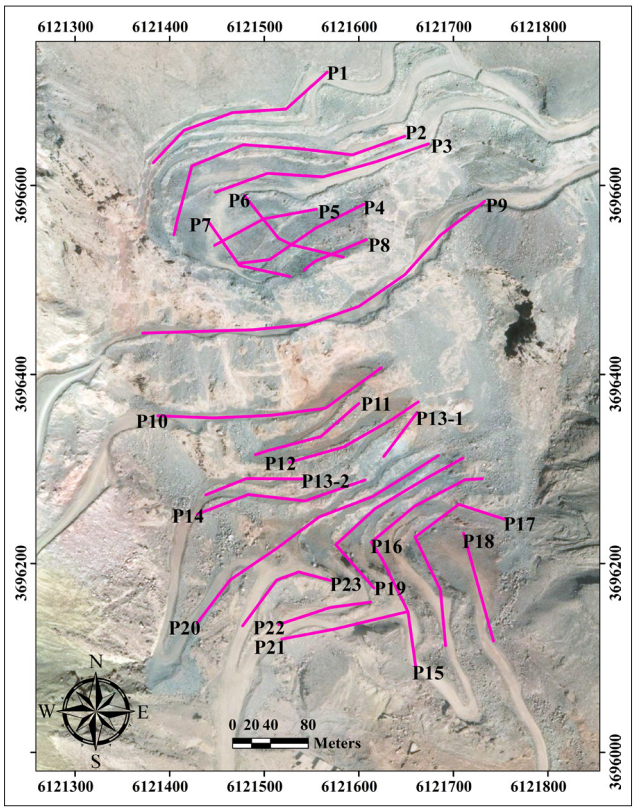

Figure 7: Locations of GPR profiles surveyed at the Mehdiabad calamine mine as shown on a Google Earth satellite image (Profile names indicate the starting location of each profile survey)

of parallel and series array configurations, with both transmitter and receiver antennas pulled consecutively along the ground surface. The total length of the 23 profiles spanned 3505 meters (see **Figure 7**). This figure depicts the locations of the GPR profiles within the Mehdiabad calamine mine. For enhanced precision, a manual GPS unit was used to record the starting, ending, and any curvature points along the survey paths. The data measurement interval along the profiles was set to 1 meter, and the total recording time window for the 25 MHz antenna was 4096 ns. Surveying primarily focused on three areas due to the presence of cliffs and steep slopes: mine terraces, berms, and a flat area in the northern part of the calamine mine. Profiles 1-3 were conducted on mine terraces, profiles 9-23 on berms, and the remaining profiles on the flat northern area (see **Figure 7**). Profile 13 required two separate surveys on distinct paths due to the risk of rockfall and potential blockage of the berm. **Figure 8** illustrates the Loza-N GPR system during data acquisition using both a 50 MHz antenna in a parallel array and a 25 MHz antenna in a series array on the terraces and berms of profile 13. Finally, **Figure 9** shows the locations of the surveyed GPR profiles superimposed on the calamine mine's geological map.

2.3.2. Data Processing

The acquired data were first processed using ReflexW 7.2 software (**URL2, 2020**). The processing steps included: Move start time, Dewow, Background removal, Gain, Butterworth band pass filter, Velocity analysis. The average velocity was determined to be 0.1 m/ns. A recorded trace (A-scan) on a radargram (B-scan) for any profile station represents the recording time in nanoseconds and the amplitudes of the reflected/diffracted electrical wavefield from discontinuities, which are characterized by vertical gradients in the dielectric permittivity. The aim of the processing is to remove noise from the radargram traces and enhance the image of the subsurface. The processed traces are displayed on the radargram with a chosen amplitude-color scale. Interpretation is then based on the variations in amplitude of the reflected/diffracted waves.

The acquired data were also processed using Krot 13.3 software (VNIISMI). This software allows for the identification of characteristic points based on phase and amplitude variations within the traces. These points are then combined to form a radar image representing the reflecting boundaries (**Buzin et al., 2017**). The traces transferred to the computer were verified using the Krot processing program, included with the instrument, to ensure the reliability of the data. The processing steps involved: Timing correction, Ormsby filter (bandpass filter), Notch filter (high-pass or low-pass filter only), Tau-P and f-K filters (used to obtain the final and residual radargrams). A static correction was applied to account for topography, allowing for its inclusion in the radargram. Final Processing Steps:

- Hodograph analysis: this involved a specific radargram obtained with common depth points (CDPs). It allows for the determination of the electromagnetic wave propagation speed and dielectric permittivity values within the subsurface.
- Deep migration and conversion: in this step, the subsurface images underwent enhancement by employing the utilized processing techniques.
- In the next step, the "Amplitude form/0" and "Amplitude form" functions were employed. These functions are capable of focusing scattered signals, collapsing hyperbolic reflections, and regulating the positioning of the reflection trend.

Generally, the electrical field recorded by the receiver includes contributions from partial reflections at vertical gradients in electrical permittivity. These reflections are represented by the amplitudes of the traces on the radargram. Characteristic points on the radargram can be interpreted as interfaces between layers with differing electrical properties. Therefore, the processed radargram provides an image of the subsurface. The amplitude and phase values on the radargram are represented by a chosen color palette. The color palette typically uses 256 levels, with different hues assigned to the maximum positive and negative polarizations, intermediate values, and zero amplitude.

Color representation in radargrams:

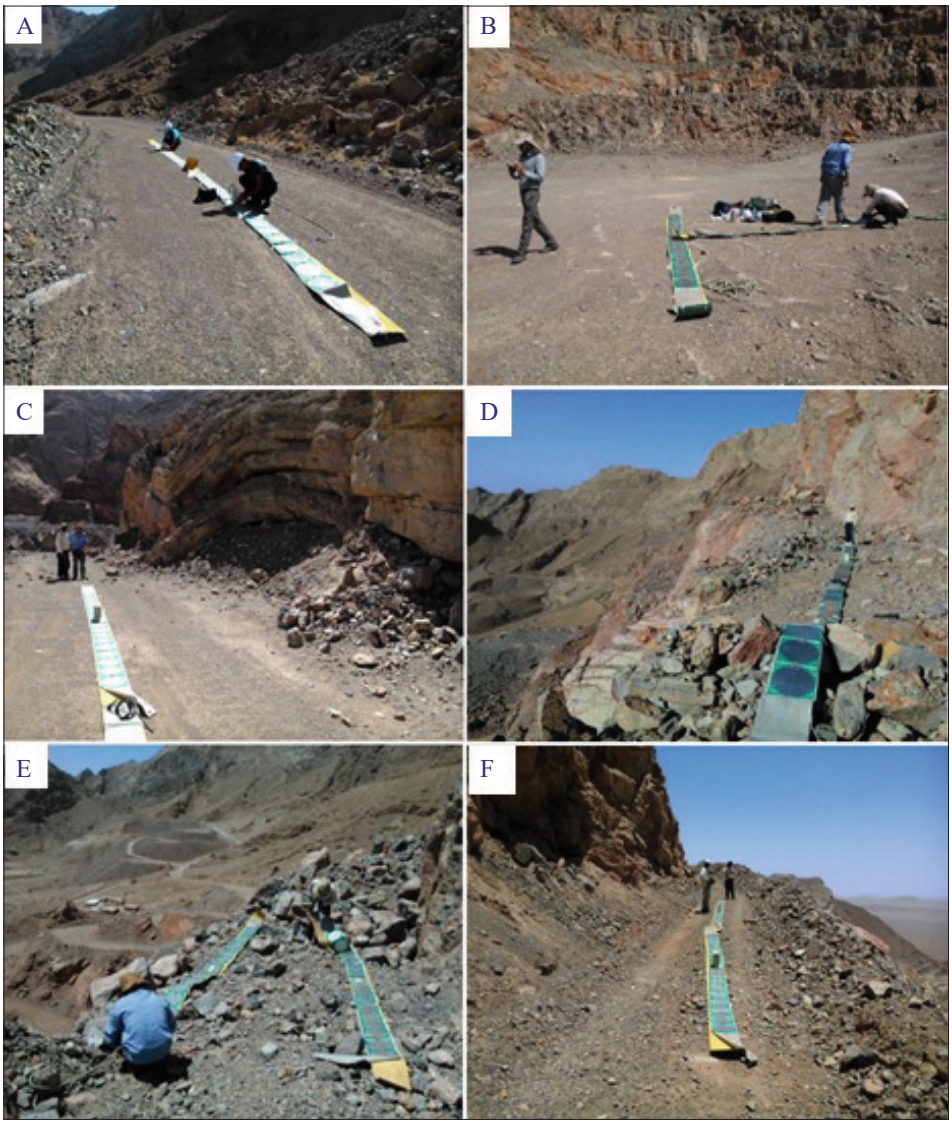

Figure 8: Loza-N DGPR profile acquisition using a system with 50 MHz and 25 MHz antennas on terraces and berms of the calamine mine. (A) Profile 22, (B) Profile 6, shown in the top-left corner of **Figure 4**, (C) Profile 16, (D) Profile 11, (E) and (F) Profile 13, surveyed in two separate sections due to rockfall.

- Positive amplitude values are displayed using a range of red hues, while negative values are depicted with shades of blue transitioning to dark blue.
- A 256-level color palette is used to represent all recorded return signal amplitudes. The lowest amplitude levels correspond to yellow tones.
- Variations in this pseudocolor scheme allow for visual representation of the entire dynamic range of amplitudes (exceeding 120 dB) and the sign of the reflected signal.

Enhanced Visualization of Weak Signals:

- The set of colors and the shape of boundaries on the radargram create an image of the geological structure obtained using the electromagnetic probing signal.
- To distinguish weak signals and improve visualization of low-contrast interfaces, we employ the "amplitude selection" method. This algorithm replaces a selected hue (e.g. one of several indistinguishable red tones) with a contrasting color, such as black.
- This replacement is applied automatically across the entire radar scan, highlighting the chosen amplitude value with the new, contrasting tone. Consequently, the selected amplitude visually represents the fine structure of variations within the reflected signal (**Prokopovich et al., 2018b**).

Software-Specific Color Palettes:

- While variations in the conventional color scheme on radargrams allowed visual representation of the entire dynamic range of GPR trace amplitudes and phases, only the boundaries between different color zones and the order of color change held geophysical meaning in Krot software.
- Conversely, ReflexW software signed all polarization values of the amplitude on the trace within the chosen color palette.

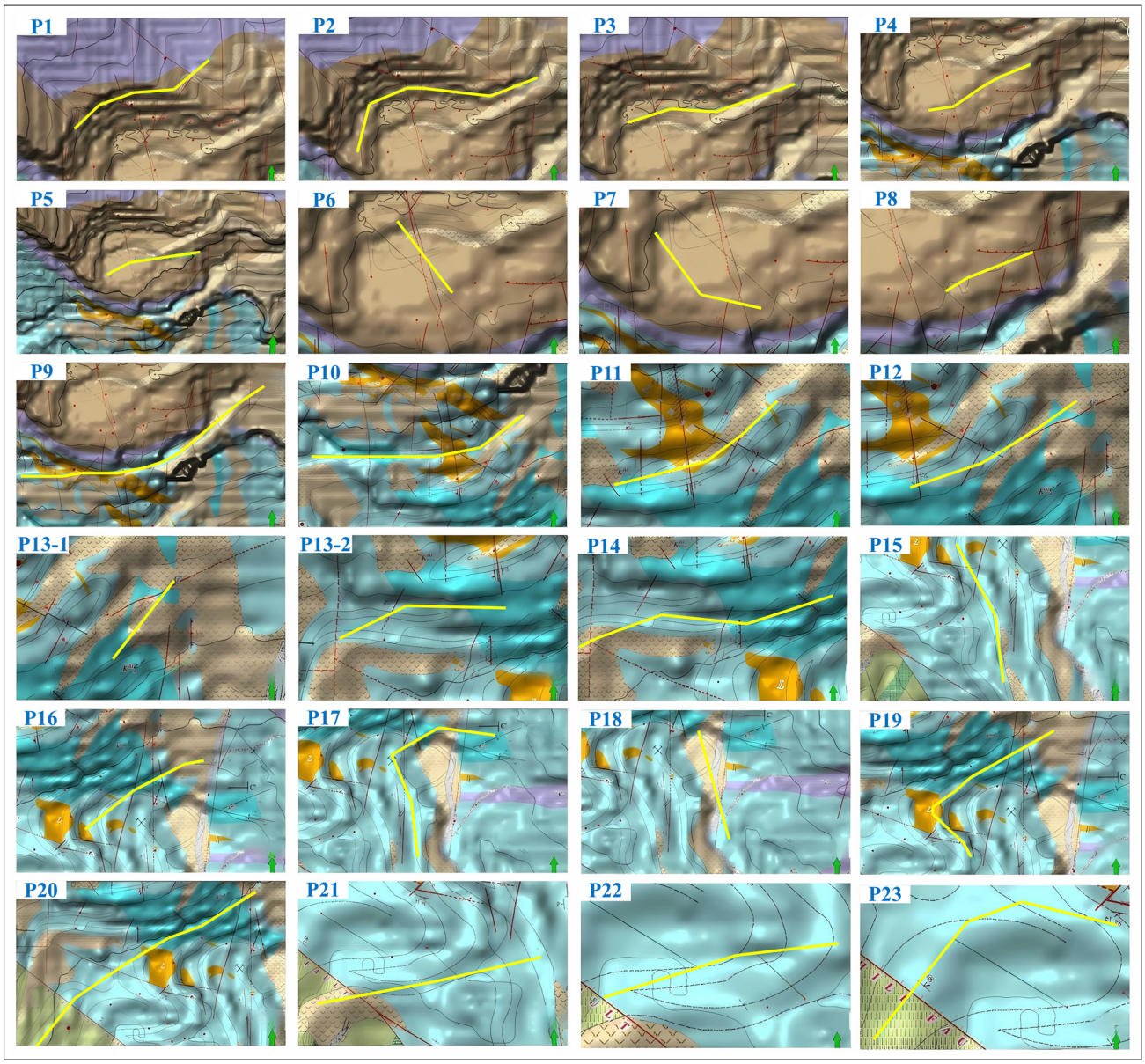

Figure 9: Locations of DGPR profiles surveyed on the calamine mine's geological map (scale 1:1,000)

Comparison of Processing Software:

- We selected radargrams from profiles including boreholes 3, 7, 9, 10, and 11. These radargrams were processed with both the linear amplitude form (representing linear vertical gradients of the electrical field) and ReflexW software.
- By comparing the processed and visualized radargrams from the same profiles using two different software packages (see **Figures 10-14**), we observed that the radargrams corroborated each other's properties.

3. Results

Profile 3, with a length of 200 meters, was surveyed on the sixth terrace of the calamine mine region. According to the geological map and schematic east-west x-section of the mine, the initial portion of this profile was surveyed on the Q^{rs} mining detritus, while the remaining portion was surveyed on the K_a^{14} limestone and dolomitic limestone units (see **Figures 3, 7, and 9**). Three main faults were identified on the radargrams (see **Figure 10**). Borehole BH7 intersected the main fault. Based on the lithology of the drilled cores and logging in borehole BH7, the following interpretations were made for the radargram (see **Figure 10a**):

- Green and light blue colors represent light green and light gray limestone containing iron oxide and calcite veins.
- Gray and yellow colors indicate light red limestone.
- A light orange color represents low-grade ore.

- An orange to red color indicates dark red marly limestone and high-grade ore.
- A dark blue color represents dark green limestone containing calcite veins.

Figures 10a and **10c** display radargrams for profile 3, which represent subsurface images. However, they differ in the way they visualize the data.

Krot's processing method (**Kopeikin et al., 2013**) utilizes both amplitude and phase information in the radargram, expressed by the equation s = vt (where s is distance, v is velocity, and t is time in nanoseconds) (see **Figure 10b**). **Figure 10b** shows the amplitude (black function) and phase (red function) of the received electrical field plotted against travel time (ns). These values are represented by a color scale with maximum, zero, and intermediate positive and negative hues. The boundaries between different hue zones and the order of color changes hold geophysical significance, reflecting variations in the subsurface.

Dielectric permittivity and conductivity are the most crucial properties influencing Ground Penetrating Radar (GPR) data. A known relationship exists between amplitude, phase, permittivity, and conductivity. Permittivity and conductivity are positively correlated, while their relationship with phase is negative. As permittivity and conductivity increase, the phase value decreases. Therefore, analyzing the phase function is crucial for interpreting the radargram.

Figure 10d displays the amplitude of the processed trace plotted against travel time (ns), again represented by a color scale. This time-domain trace depicts reflected and diffracted electrical fields. This explains the visual differences between **Figures 10a** and **10d**.

Figure 10a can depict subsurface layers with both vertical and lateral variations, providing insight into the relative permittivity of these layers. **Figure 10d**, on the other hand, primarily visualizes approximately horizontal reflection layers. Vertical variations can still be inferred from the amplitudes of diffracted signals. Profile P7, with a length of 96 meters and a northwest-southeast strike, was surveyed on the northern flat part of the calamine mine. The underlying geology consists of limestone and dolomitic limestone units (K_a^{14}) (see **Figures 3, 7,** and **9**). Two main faults were identified on the radargram (see **Figure 11**). Boreholes BH8 and BH11 were drilled along this profile. Based on the lithology (rock types) of the drilled cores and well logging data from boreholes BH8 and BH11, the colors in radargram (see **Figure 11a**) can be interpreted as follows:

- Green and light blue colors represent light green and light gray limestone containing iron oxide and calcite veins.
- Gray and yellow colors indicate light gray limestone.
- A light orange color represents low-grade ore.

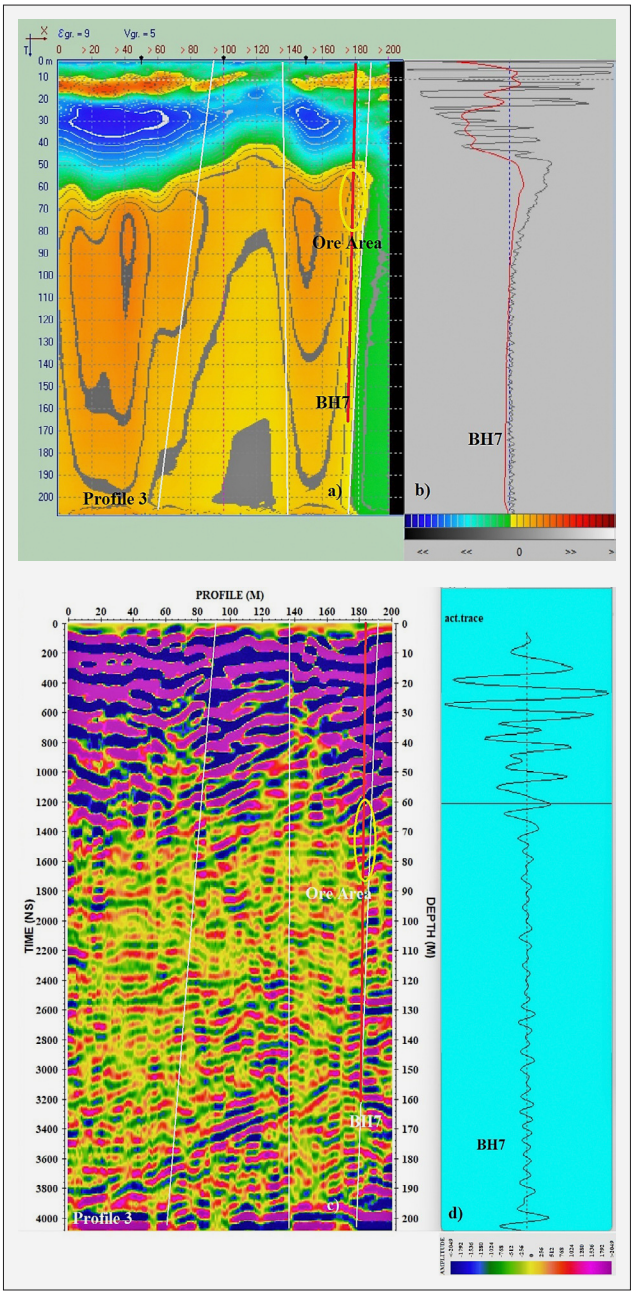

Figure 10: Radargrams of the profile 3 processed with (a) Krot, (c) ReflexW displayed by linear amplitude form/o filter. The white lines represent identified macro faults. The red line indicates the location of borehole BH7, and the yellow circle highlights the zone interpreted as ore based on data from BH7.

- An orange to red color indicates dark red marly limestone and high-grade ore.
- A dark blue color represents dark green limestone containing calcite veins.

As observed in **Figures 10a, 10b, 11a, and 11b** the layer represented by dark blue hues has the lowest dielectric permittivity. Layers of light green and light gray limestone with iron oxide and calcite veins (represented by light blue and green hues) have a lower permittivity compared to the layers of dark red marly limestone and

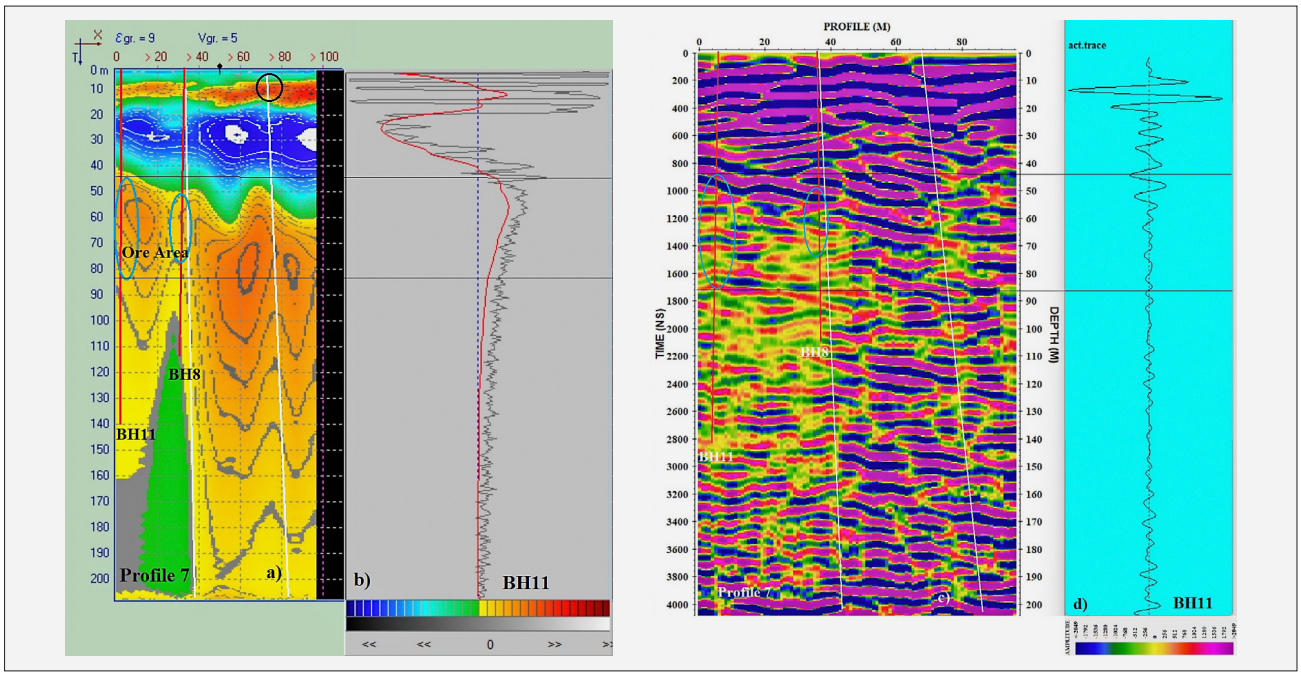

Figure 11: Radargrams of the profile 7 processed with (a) Krot, (c) ReflexW displayed by linear amplitude form/o filter. The white lines represent macro faults, while the red lines indicate the locations of boreholes BH8 and BH11. The black circles show excavation sites, and the blue circles highlight the main ore zones identified in boreholes BH8 and BH11.

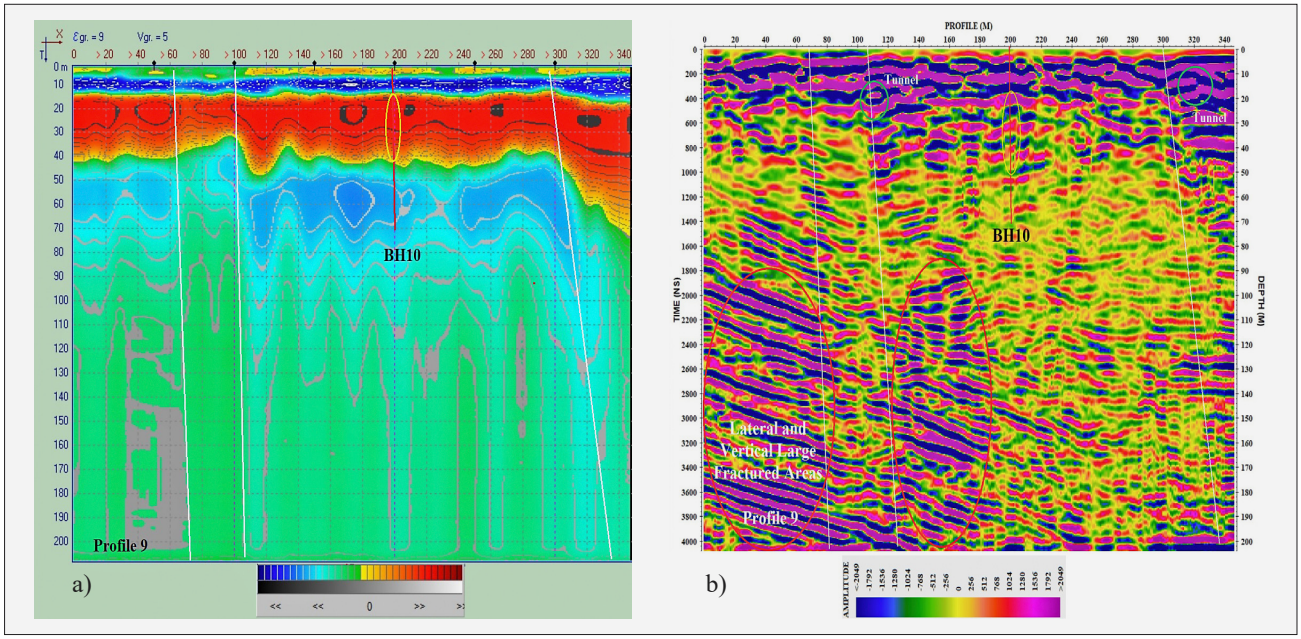

Figure 12: Radargrams of the profile 9 processed with (a) Krot, (b) ReflexW displayed by linear amplitude form/o filter. The white lines represent macro faults. The red line indicates the location of borehole BH10. Green circles highlight known cavities and tunnels based on information from old mine maps. The yellow circle highlights the main ore zone identified in borehole BH10.

high-grade ore. This is likely because the iron oxide in the lighter-colored layers influences their permittivity.

Profile 9, the longest GPR profile surveyed on the mine, measured 346 meters in length with a northeast-southwest strike. It followed the main access road to lens number 2 on the calamine mine's geological map (see **Figure 3**). The profile can be divided into distinct geological sections:

- The first 145 meters: traversed Q^{rs} mining detritus.
- The next 82 meters (from 145 to 227 meters): crossed the thick-bedded and massive K_a^{12} reefal limestone unit.

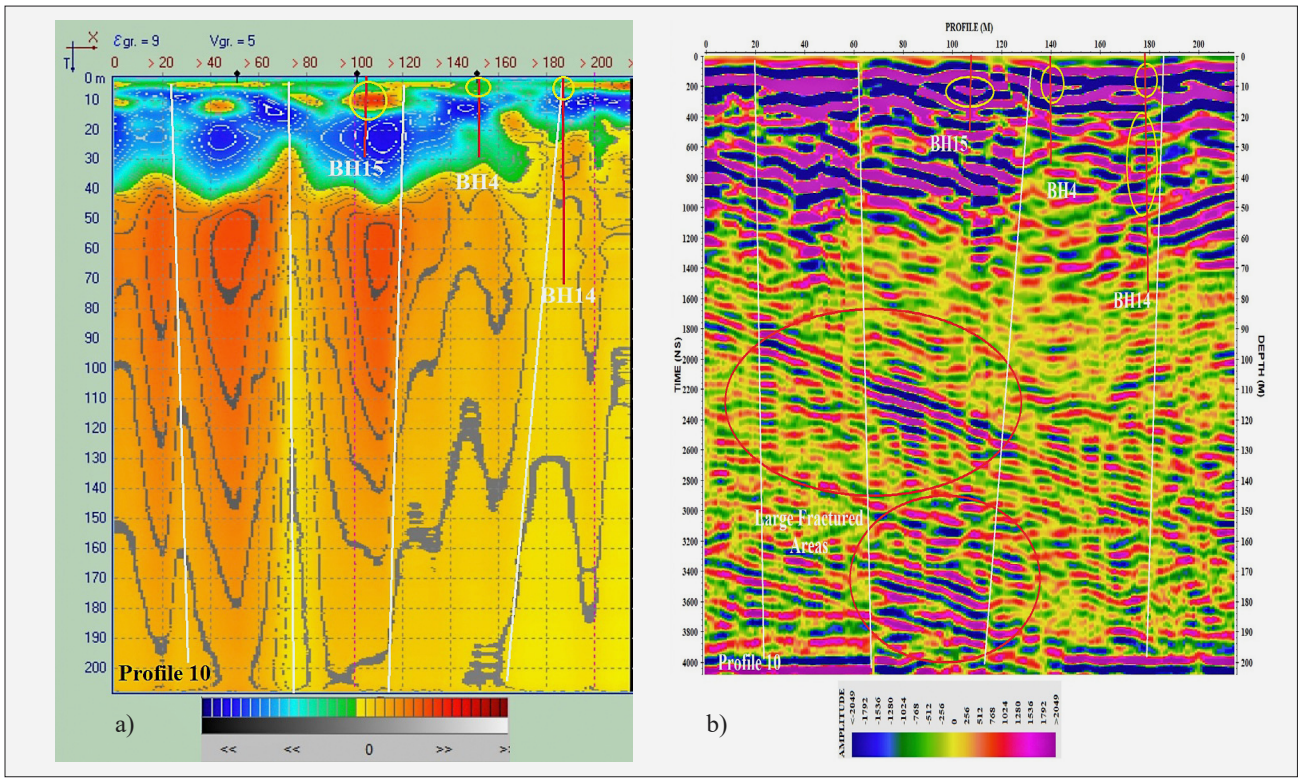

Figure 13: Radargrams of the profile 10 processed with (a) Krot, (b) ReflexW displayed by linear amplitude form/o filter. The white lines represent macro faults. The red lines indicate the locations of boreholes BH4, BH14, and BH15. The yellow circles highlight the main ore zones identified in boreholes BH4, BH14, and BH15. The red circles depict large fractured areas.

- The following 95 meters (from 227 to 322 meters): entered the lead and zinc calamine mineralization zone, known as lens number 2 on the geological section (see **Figures 5B** and **9**).
- The remaining 24 meters of profile 9: remained on the K_a^{12} unit (**Figure 9**).

Three right strike-slip faults were identified on the radargrams in **Figure 12**. Based on the drilled core lithology and well logging data from borehole BH10, the colors in radargram (see **Figure 12a**) can be interpreted as follows:

- Green and light blue colors represent light green and light gray limestone containing iron oxide and calcite veins (based on well logging observations).
- Gray and yellow colors indicate light gray limestone.
- A light orange color represents low-grade ore as observed in the drilled core.
- An orange to red color indicates dark red marly limestone and high-grade ore.
- A dark blue color represents dark green limestone containing calcite veins (based on the drilled core).

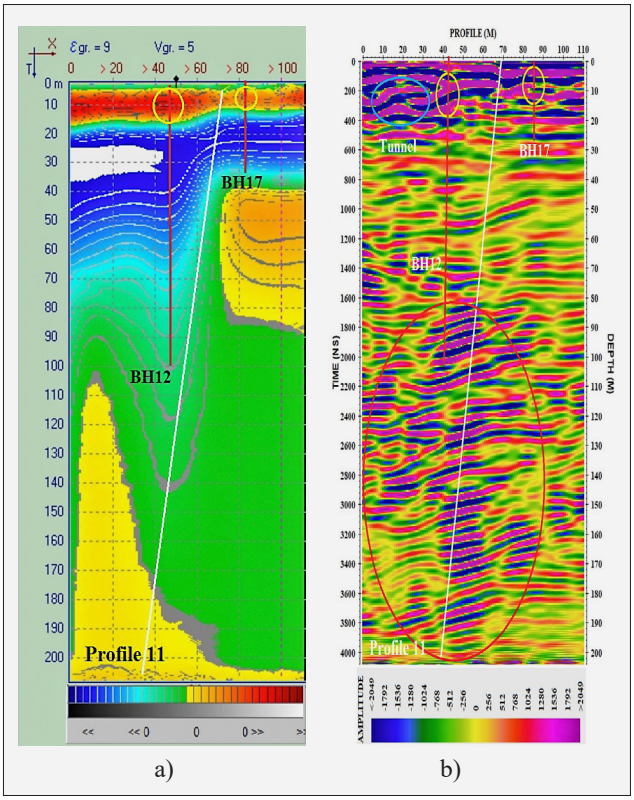

Figure 14: Radargrams of the profile 11 processed with (a) Krot, (b) ReflexW displayed by linear amplitude form/o filter. The white lines represent macro faults. The red lines indicate the locations of boreholes BH12 and BH17. The yellow circles highlight the main ore zones identified in the boreholes. The blue circle highlights an excavation tunnel based on information from old mine maps. Finally, the red circle depicts a large fractured area within the profile. ➤

The radargram in **Figure 12a** suggests high-grade ore zones at depths between 12-14 meters and 35-48 meters. The red-colored section between 15-35 meters likely represents fresh dark green limestone with calcite veins. These interpretations support the layer identifications made in **Figures 10** and **11**. However, the radargram in **Figure 12b** is inconclusive for the left section beyond 200 meters. It cannot determine the presence or absence of stability problems in that area. The results from profile 9 indicate the presence of high-grade ore at an approximate depth of 15-40 meters.

Profile P10, with a west-east strike, was surveyed along the access road to lens number 2 of the calamine mine (see **Figures 3, 7,** and **9**). According to the geological section, the profile traverses distinct geological units:

- The initial 41 meters: lie on K_a^{12} limestone and dolomitic units.
- The next 34 meters (from 41 to 75 meters): cross K_a^{sh1} gray to dark gray shaly limestone and cherty dolomitic units. These units are expected to have a reduced wave amplitude in the radargram.
- Between 75 and 120 meters: the profile overlies lens number 2.
- The remaining portion of the profile: crosses both K_a^{12} and Q^{rs} lithologic units (see **Figures 3, 7,** and **9**).

The resulting radargrams for profile 10 (see **Figure 13**) indicate:

- **Figure 13a**: the boundaries of limestone with varying degrees of mineralization.
- **Figure 13b**: the presence and location of fracture zones with high accuracy.

Boreholes BH4, BH14, and BH15 support the layer identifications established in other profiles.

Profile 11, with an east-west strike, was surveyed along the southern edge of the lens 2 outcrop at the calamine mine (see **Figures 3** and **9**). The profile traverses the following geological units:

- The first 12 meters: overlay the K_a^{12} rock unit.
- From 12 to 38 meters: it crosses the Q^{rs} unit.
- The next section, from 38 to 72 meters: lies on calamine lens 2.
- The remaining part of the profile: overlies a combination of Q^{rs} and K_a^{12} lithologic units on the surface.

As in previous profiles, the radargram (see **Figure 14a**) suggests:

- An orange color: represents high-grade ore zones.
- A yellow color: represents low-grade ore zones.

The presence of excavation tunnels is indicated by the blue circles beneath the profile. The radargram also reveals:

- A major normal fault and large vertical fractures exceeding 80 meters in depth (see **Figure 14b**).

Figure 14 offers an intriguing view of the tectonic structure:

- The normal fault is clearly visible.

This fault appears to connect with a large fracture zone starting at a depth of 80 meters.

4. Discussion

The Ground Penetrating Radar (GPR) method offers superior resolution compared to other geophysical techniques for shallow investigations. However, its penetration depth is significantly limited by the dielectric permittivity and conductivity of the subsurface environment. To overcome these limitations, the use of GPR devices from the Loza series is recommended. The choice of Loza series GPR device for a particular application depends on the required survey depth, geological conditions, and environmental factors. Di Marzo et al. (2018) categorized Loza series antennas into four main types:

- Low-frequency antennas: these antennas operate at lower frequencies (typically below 100 MHz) and are designed for deep penetration, reaching depths of up to 200 meters or more in favorable conditions. They are well-suited for geological surveys, groundwater exploration, and archeological investigations.
- Medium-frequency antennas: these antennas operate in the mid-frequency range (100 MHz to 500 MHz) and offer a balance between penetration depth and resolution. They are suitable for a wider range of applications, including utility mapping, environmental site assessments, and infrastructure inspections.
- High-frequency antennas: these antennas operate at higher frequencies (above 500 MHz) and provide high-resolution images of near-surface features. They are commonly used for concrete inspection, pavement evaluation, and shallow soil surveys.
- Multi-frequency antennas: these antennas combine multiple frequency bands into a single unit, offering a broader range of penetration and resolution capabilities. They are versatile tools for applications that require detailed information at varying depths.

The choice of antenna should be made in consultation with an experienced GPR professional who can assess the specific requirements of the project and recommend the most appropriate Loza series device. To explore deeper mineralized zones and faults in the Mehdiabad calamine mine, a new system with a 25 MHz antenna called Loza-N DGPR was employed. This system was specifically chosen due to its theoretical penetration depth of approximately 200 meters. The effectiveness of the 25 MHz antenna for achieving this depth was evaluated in the field. Data processing was performed using ReflexW and Krot software, yielding promising results. While the software produced images with distinct characteristics, both indicated successful penetration up to 200 meters.

The radargrams obtained using Krot software effectively distinguished limestone units based on a selected

amplitude and phase color scale. The accuracy of these identifications was confirmed by borehole data. While both 25 MHz and 50 MHz antennas were used for data collection on 23 profiles, only the 25 MHz Loza radargrams are presented in this paper. This choice aligns with the study's primary objective: identifying mineralized zones and faults. In a mining context, pinpointing ore locations with depth variations is crucial for informed decision-making. The processed radargrams from ReflexW successfully achieved this goal by mapping the two-dimensional distribution of high-grade and low-grade ore at varying depths. Furthermore, these radargrams, along with processing by ReflexW, facilitated the mapping of faults and fractures within the mine. This comprehensive data allows mine management to more readily make informed decisions. It is noteworthy that achieving favorable results in the ReflexW environment is contingent upon data acquisition using the Loza-N device, which boasts enhanced penetration depth and resolution of subsurface structures. Additionally, the data processing results exhibit concordance between the two software packages. **Figure 10** depicts Profile 3 with an east-west trend. **Figure 11** illustrates Profile 7 with a northwest-southeast trend. Both profiles were acquired on the K_a^{14} rock unit. Mineralization was identified at the end of Profile 3 at 180 meters and at the beginning of Profile 7 at 6 and 36 meters in the DGPR radargrams. The mineralized zones overlap based on the end of Profile 3 and the beginning of Profile 7. Additionally, studies of drill cores have confirmed the continuity of the mineralized zones by examining the attached geological logs.

Another significant finding pertains to the relationship between permittivity and layer units. The presence of calcite veins and iron oxide increases permittivity and decreases the phase of the GPR signal. Despite this influence, the GPR wave successfully penetrated up to 200 meters using the Loza-N DGPR system, demonstrating its effectiveness in this specific geological context.

5. Conclusions

The radargrams processed using ReflexW software effectively revealed bedding structures within the subsurface layers down to a depth of 200 meters. Additionally, the boundaries and locations of faulted zones identified on the 25 MHz Krot software radargrams showed excellent agreement with the existing geological map of the area.

In sections consisting solely of pure limestone, the electromagnetic waves achieved a maximum penetration depth of 200 meters with minimal energy loss. In this context, dark orange to red color zones can be observed in the radargrams of Section a in **Figures 10, 11,** and **13**, which represent high-grade zones based on the study of drilled cores on the proposed DGPR profiles. However, the wave amplitude was observed to decrease in zones where limestone units contained shale or had undergone dolomitization. This same effect was observed in areas with faults due to the crushed and brecciated nature of the rock units. By examining the petrography of drilled cores and the logs obtained from the drilled boreholes, it can be inferred that the green and light blue to dark blue color zones in the radargrams represent, respectively, zones containing iron oxide and calcite veins. In general, in these zones, wave attenuation has increased and electromagnetic signals have weakened. The Loza-N DGPR system demonstrated several key advantages:

- High Penetration Depth: the system achieved successful penetration of up to 200 meters in the specific geological conditions of the mine.
- Detailed Geological Mapping: the DGPR data facilitated the clear identification of rock units within the surveyed area, particularly differentiating pure limestone from shale-bearing limestone and dolomitic limestone units.
- Low Noise Data: the DGPR method yielded data with minimal noise levels, enhancing the interpretability of the results.

Based on the positive outcomes achieved in this study, employing the DGPR method for further exploration in other parts of the Mehdiabad mine is highly recommended.

Acknowledgements

This research was conducted as part of the senior author's Master's thesis at Kharazmi University, Tehran, Iran. The authors would like to express their gratitude to Kharazmi University and Ankara University for their support. We are particularly grateful to the board of the Mehdiabad Mining Complex, especially M. Hajighasemi and A. Safari, for granting us access to the deposit and providing valuable exploration data, core logs, maps, and historical records. Their cooperation was instrumental in the successful completion of this study.

7. References

Akyüz, H.S., Kırkan, E., Basmenji, M., Aksoy, E., Akyüz, A. D., Uçarkuş, G., Yazıcı, M., Yakupoğlu, N., Zabcı, C. (2019): Paleoseismological and Morphotectonical Characteristics of Active Faults in the Vicinity of Muğla Area (SW Turkey). 1st Springer Conference of the Arabian Journal of Geosciences, Volume: On Significant Applications of Geophysical Methods, Advances in Science, Technology & Innovation. 253-256. https://doi.org/10.1007/978-3-030-01656-2_57

Aliyannezhadi, A., Mehrnia, S.R., Kimiagar, S., Rahimi, H., Sadrmohammadi, N. (2020): Evaluation of GPR method in identification hidden faults of Alluvial deposits in north of Persian Gulf artificial lake, twenty-two district of Tehran. Journal of Applied Geophysics. 179, 1-12. https://doi.org/10.1016/j.jappgeo.2020.104108

Baggett, J., Abbasi Baghbadorani, A., Monsalve, J., Edwin Bishop, R., Ripepi, N., Hole, J. (2019): Ground-Penetrating Radar for Karst Detection in Underground Stone Mines. Mining Metallurgy & Exploration. 37 (2), 1-13. https://doi.org/10.1007/s42461-019-00144-1

Berkut, A.I., Edemsky, D.E., Kopeikin, V.V., Morozov, P.A., Prokopovich, I.V., Popov, A.V. (2017): Deep penetration subsurface radar: Hardware, results, interpretation. 9th International Workshop on Advanced Ground Penetrating Radar (IWAGPR), Edinburgh, UK. http://dx.doi.org/10.1109/IWAGPR.2017.7996052

Borg, G. (2005): Geological and economical significance of supergene nonsulphide zinc deposits in Iran and their exploration potential. In: Geological Survey of Iran (Ed.) Mining and Sustainable Development. 20th World Mining Congress, Tehran, Iran. 7-11.

Brandes, Ch., Igel, J., Loewer, M., Tanner, D.C., Lang, J., Müller, K., Winsemann, J. (2018): Visualisation and analysis of shear-deformation bands in unconsolidated Pleistocene sand using ground-penetrating radar: Implications for paleoseismological studies. Sedimentary Geology. 367, 135-145. https://doi.org/10.1016/j.sedgeo.2018.02.005

BRGM (1994): Mehdiabad lead-zinc deposit pre-feasibility study. Geological assessment report N1392, May, BRGM Department Exploration BP 600945060 Orleans Cedex, France.

Buzin, V., Edemskij, D., Gudoshnikov, S., Kopeikin, V., Morozov, P., Popov, A., Prokopovich, I., Skomarovskij, V., Melnik, N., Berkut, A., Merkulov, S., Vorovskij, P., Bogolubov, L. (2017): Search for Chelyabinsk Meteorite Fragments in Chebarkul Lake Bottom (GPR and Magnetic Data). Journal of Telecommunications and Information Technology. 3, 69-78. https://doi.org/10.26636/jtit.2017.120817

Daniels, J.J. (1989): Fundamentals of ground penetrating radar Symposium on the Application of Geophysics to Environmental and Engineering Problems (SAGEEP'89) Proc. Environmental and Engineering Geophysical Society (Englewood, Colorado). 62-142.

Davis, J.L., Annan, A.P. (1989): Ground-penetrating radar for high resolution mapping of soil and rock stratigraphy. Geophysical Prospecting. 37, 531-551. http://dx.doi.org/10.1111/j.1365-2478.1989.tb02221.x

Di Marzo, G., Falcucci, M., Lambiris, R. (2018). GPR antennas for deep exploration: A review. Journal of Archaeological Science: Reports, 18, 22-37.

Ebrahim Mohseni, M. (2011): Study of genesis of Mehdiabad deposit using fluid inclusion and stable isotope. [Unpublished M.Sc. Thesis], Damghan University, Damghan, Iran, 166 p.

Elkarmoty, M., Colla, C., Gabrielli., C., Kasmaeeyazdi., S., Tinti, F., Bonduà, S., Bruno, R. (2017): Mapping and modelling fractures using ground penetrating radar for ornamental stone assessment and recovery optimization: Two case studies. Rudarsko-geološko-naftni zbornik. 32 (4), 63-76. https://doi.org/10.17794/rgn.2017.4.7

Francke, J., Utsi, V., (2009): Advances in long-range GPR systems and their applications to mineral exploration, geotechnical and static correction problems. First Break. 27 (7), 85-93. https://scholar.google.com/citations?user=V2W5LIEAAAAJ&hl=en

Francke, J. (2010): Applications of GPR in Mineral Resource Evaluations. IEEE, Conference Location: Lecce, Italy. https://doi.org/10.1109/ICGPR.2010.5550188

Ghasemi, M. (2006): Formation Mechanism of the Mehdi Abad Zn–Pb Deposit and its Comparison with Other Near Lead and Zinc Deposits. [Unpublished M.Sc. Thesis], Research Institute of Earth Sciences, Geological Survey and Mineral Exploration of Iran, Iran, 238 p.

Gu, Zh., Shi, Ch., Yang, H., Yao, H. (2018): Analysis of dynamic sedimentary environments in alluvial fans of some tributaries of the upper Yellow River of China based on ground penetrating radar (GPR) and sediment cores. Quaternary International. 509, 30-40. https://doi.org/10.1016/j.quaint.2018.05.001

Hashemi Marand, G., Jafari. M., Afzal. P., Khakzad. A. (2018): Determination of relationship between silver and lead mineralization based on fractal modeling in Mehdiabad Zn-Pb-Ag deposit, Central Iran. Journal of Earth Sciences. 27, 111-118. https://doi.org/10.22071/gsj.2018.58371

He, F.B., Bai, L.Y., Wang, J.M., Liu, Y. (2013): Deep structure and Quaternary activities of the Xiadian fault zone. Seismology and Geology. 35 (3), 490-505. (In Chinese with English Abstract).

Kadioglu, S., Ulugergerli, E.U. (2012): Imaging karstic cavities in transparent 3D volume of the GPR data set in Akkopru dam, Mugla, Turkey. Nondestructive Testing and Evaluation. 27 (3), 263- 271. http://dx.doi.org/10.1080/10589759.2012.694885

Kadioglu, S., Daniels, J.J. (2008): 3D visualization of integrated ground penetrating radar data and EM-61 data to determine buried objects and their characteristics. Journal of Geophysics and Engineering. 5 (4), 448-456. https://doi.org/10.1088/1742-2132/5/4/008

Kadioglu, S., Kadioglu, M., Kadioglu, Y.K. (2013a): Identifying of buried archaeological remains with ground penetrating radar, polarized microscope and confocal Raman spectroscopy methods in ancient city of Nysa, Aydin - Turkey. Journal of Archaeological Science. 40 (10), 3569-3583. https://doi.org/10.1016/j.jas.2013.04.001

Kadioglu, S., Kadioglu, Y.K., Catapano, I., Soldovieri, F. (2013b): Ground penetrating radar and microwave tomography for the safety management of a cultural heritage site: Miletos Ilyas Bey Mosque (Turkey). Journal of Geophysics and Engineering. 10 (6), 064007 (11 p). https://doi.org/10.1088/1742-2132/10/6/064007

Kadioglu, S., Kadioglu, Y.K. (2016): Visualization of buried anti-tank landmines and soil pollution: analyses using ground penetrating radar method with attributes and petrographical methods. Near Surface Geophysics. 14 (2), 183-195. https://doi.org/10.3997/1873-0604.2016010

Kadioglu, S. (2018): Research of the sea-filled airport OGU in the Black Sea, Turkey, using ground penetrating radar method. Construction and Building Materials. 158 (15), 1123-1133. https://doi.org/10.1016/j.conbuildmat.2017.09.055

Kofman, L., Ronen, A., Frydman, S. (2006): Detection of model voids by identifying reverberation phenomena in

GPR records. Journal of Applied Geophysics. 59 (4), 284-299. https://doi.org/10.1016/j.jappgeo.2005.09.005

Kopeikin, V.V., Edemsky, D.E., Garbatsevich, V.A., Popov, A.V., Reznikov, A.E., Schekotov, A.Yu. (1996): Enhanced power ground penetrating radars, in Proceedings of 6th International Conference on Ground Penetrating Radar, Sendai, Japan, 152-154.

Kopeikin, V.V., Morozov, P.A., Edemskiy, F.D., Edemskiy, D.E., Pavlovskii, B.R., Sungurov, Yu.A. (2012): Experience of GPR application in oil-and-gas industry. 14th International Conference on Ground Penetrating Radar (GPR). Shanghai, China, 1-5. https://doi.org/10.1109/ICGPR.2012.6254973

Kopeikin, V.V., Kuznetsov, V.D., Morozov, P.A., Popov, A.V., Berkut, A.I., Merkulov, S.V., Alexeev, V.A. (2013): Ground Penetrating Radar Investigation of the Supposed Fall Site of a Fragment of the Chelabinsk Meteorite in Lake Chebarkul'. 51 (7), 575-582. https://doi.org/10.1134/S0016702913070112

Liang, K., Ma, B., Li, D., Tian, Q., Sun, Ch., He, Zh., Zhao, J., Liu, R., Wang, J. (2019): Quaternary activity of the Zhuozishan West Piedmont Fault provides insight into the structural development of the Wuhai Basin and Northwestern Ordos Block, China. Tectonophysics. 754, 56- 72. https://doi.org/10.1016/j.tecto.2019.02.004

Lunina, O.V., Gladkov, A.S., Gladkov, A.A. (2018): Surface and shallow subsurface structure of the Middle Kedrovaya paleoseismic rupture zone in the Baikal Mountains from geomorphological and ground-penetrating radar investigations. Geomorphology. 326, 54-67. https://doi.org/10.1016/j.geomorph.2018.03.009

Luoma, S., Majaniemi, J., Nurminen, T., Pasanen, A. (2016): GPR survey and field work summary in Siilinjärvi Mine during July 2014, Geological Survey of Finland. Archive report, 66.

Maghfouri, S. (2017): Geology, Geochemistry, Ore Controlling Parameters and Genesis of Early Cretaceous Carbonate-clastic Hosted Zn-Pb Deposits in Southern Yazd Basin, with Emphasis on Mehdiabad Deposit. [Unpublished Ph.D. Thesis], Tabriz University, Iran, 475 p.

Maghfouri, S., Hosseinzadeh, M.R., Choulet, F., Alfonso, P., Azimzadeh, A.M., Rajabi, A. (2019): Vent-proximal subseafloor replacement clastic-carbonate hosted SEDEX-type mineralization in the Mehdiabad world-class Zn-Pb-Ba-(Cu-Ag) deposit, southern Yazd Basin, Iran. Ore Geology Reviews. 113, 103047. https://doi.org/10.1016/j.oregeorev.2019.103047

Manu, E., Preko, K., Wemegah, D.D. (2013): Application of Ground Penetrating Radar in delineating zones of Gold Mineralization at the Subenso-North Concession of Newmont Ghana Gold Limited. International Journal of Scientific and Research Publication. 3 (5), 1-11.

Morozov, P., Morozov, F., Lazarev, M., Bogolyubov, L., Popov, A. (2023): Characterization of Antenna Radiation Pattern and Penetration Depth in Ground Penetrating Radar Field Missions. remote sensing. 15 (23). https://doi.org/10.3390/rs15235452

Nakanishi, T., Takemura, K., Matsuyama, H., Shimoyama, Sh., Hong, W., Okuno, M. (2017): Activity of the Funai Fault and Radiocarbon Age Offsets of Shell and Plant Pairs from the Latest Pleistocene to Holocene Sediments Beneath the Oita Plain, Western Japan. Radiocarbon. 59 (6), 1737-1748. https://doi.org/10.1017/RDC.2017.119

Patterson, J.E., Cook, F.A. (2002): Successful application of ground-penetrating radar in the exploration of gem tourmaline pegmatites of southern California. Geophysical Prospecting. 50 (2), 107-117. http://doi.org/10.1046/j.1365-2478.2002.00312.x

Prokopovich, I., Popov, A., Pajewski, L., Marciniak, M. (2018a): Application of Coupled-Wave Wentzel-Kramers-Brillouin Approximation to Ground Penetrating Radar. Remote sensing. 10 (22), 1-20. http://doi.org/10.3390/rs10010022

Prokopovich, I.V., Morozov, P.A., Popov, A.V., Kopeikin, V.V., Berkut, A.I., Krinitsky, L.M. (2018b): Deep Penetration Radar: Hydrogeology and Paleorelief of Underlying Medium. 17th International Conference on Ground Penetrating Radar (GPR). Rapperswil, Switzerland, 1-5. https://doi.org/10.1109/ICGPR.2018.8441525

Popov, A., Berkut, A., Edemsky, D., Kopeikin, V., Morozov, P., Prokopovich, V. (2017): Deep Penetration Subsurface Radar: Hardware, Results, Interpretation. 9th Internat. Workshop on Advanced Ground Penetrating Radar, pp. 117-122. Edinbourgh, UK. https://doi.org/10.1109/IWAGPR.2017.7996052

Pupatenko, V.V., Sukhobok, Y.A., Stoyanovich, G.M. (2017): Lithological Profiling of Rocky Slopes Using GeoReader Software Based on the Results of Ground Penetrating Radar Method. Procedia Engineering. 189, 643 – 649. https://doi.org/10.1016/j.proeng.2017.05.102

Pupatenko, V., Sukhobok, Y., Stoyanovich, G., Stetsyuk, A., Verkhovtsev, L. (2019): GPR data interpretation in the landslides and subgrade slope surveys. International Geotechnical Symposium "Geotechnical Construction of Civil Engineering & Transport Structures of the Asian-Pacific Region" (GCCETS 2018). 265, 1-6. https://doi.org/10.1051/matecconf/201926503003

Pourfaraj, H. (2016): Structural analysis of fault systems in Mehdiabad Zn-Pb Mine area, SE Yazd. [Unpublished M. Sc. Thesis], Tarbiat Modares University, Iran, 192 p.

Ralston, J.C., Strange, A.D. (2015): An industrial application of ground penetrating radar for coal mining horizon sensing. International Symposium on Antennas and Propagation (ISAP), Hobart, TAS, Australia.

Reichert, J. (2007): A Metallogenetic Model for Carbonate hosted Non-sulfide Zinc Deposits Based on Observations of Mehdi Abad and Iran Kouh, Central and Southwestern Iran. [Unpublished Ph.D. Thesis], University of Martin Luther, Shillong, 129 p.

Reichert, J., Borg, G., Rashidi, B. (2003); Mineralogy of calamine ore from the Mehdi Abad zinc-lead deposit, Central Iran. Conference 7th Biennial Meeting, Society for Geology Applied to Mineral Deposits; Mineral exploration and sustainable development, Athens. 97-102.

Rehman, Q.U., Ahmed, W., Waseem, M., Khan, S. (2021): Geophysical investigations of a potential landslide area in Mayoon, Hunza District, Gilgit-Baltistan, Pakistan. Ru-

darsko-geološko-naftni zbornik. 36 (3), 127-141. https://doi.org/10.17794/rgn.2021.3.9

Rezaei, A., Hassani, H., Moarefvand, P., Golmohammadi, A. (2019): Determination of unstable tectonic zones in C-North deposit, Sangan, NE Iran using GPR method: importance of structural geology. Journal of Mining and Environment. 10 (1), 177-195. https://doi.org/10.22044/jme.2019.7378.1590

Sadrmohammadi, N., Mehrnia, S.R., Rezaei, Kh., Kadioğlu, S., Honarvar, M. (2021): Evaluation of Fractal Variance-Distance Model in Identifying Geochemical Anomalies of Calamine Mehdiabad Mining Complex, Central Iran. Journal of Mining and Environment. 12 (1), 45-62. https://doi.org/10.22044/jme.2020.10215.1960

Singh, K.K.K., Chauhan, R.K.S. (2002): Exploration of subsurface strata conditions for a limestone mining area in India with ground-penetrating radar. Environmental Geology. 41, 966-971. https://doi.org/10.1007/s00254-001-0475-x

Stemberk, J., Dal-Moroa, G.C., Stemberka, J., Blahůta, J., Coubala, M., Košťáka, B., Zambranob, M., Tondib, E. (2019): Strain monitoring of active faults in the central Apennines (Italy) during the period 2002–2017. Tectonophysics. 750, 22–35. https://doi.org/10.1016/j.tecto.2018.10.033

Stöcklin, J. (1968): Structural history and tectonics of Iran; a review, American Association of Petroleum Geologists Bulletin, 52 (7), 1229-1258.

Wong, I., Thomas, P., Koehler, R., Lewandowski, N. (2019): Assessing the Seismic Hazards in Jamaica Incorporating Geodetic and Quaternary Fault Data. Bulletin of the Seismological Society of America. 109 (2), 716-731. https://doi.org/10.1785/0120180205

Xu, X., Peng, S., Yang, F. (2018): Development of a ground penetrating radar system for large-depth disaster detection in coal mine. Journal of Applied Geophysics. 158, 41-47. https://doi.org/10.1016/j.jappgeo.2018.07.006

Zanzi, L., Hojat, A., Ranjbar, H., Karimi Nasab, S. (2017): GPR measurements to detect major discontinuities at Cheshmeh-Shirdoosh limestone quarry, Iran. Bulletin of Engineering Geology and the Environment. 78, 743-752. https://doi.org/10.1007/s10064-017-1153-x

Zhao, Y., Cai, X.M., Wang, J.M., Zhang, L., Liu, Y., Lv, J.B. (2015): The division of "small blocks" of structure in Beijing plain and a discussion on the activity of micro block in Quaternary period. Geology in China. 42 (6), 1876-1884.

URL1: https://www.geonica.com/en/georadar.php, (accessed 12th April 1996).

URL2: https://www.sandmeier-geo.de/ (accessed 24th August 2020).

SAŽETAK

Snimanje podzemlja georadarom u svrhu istraživanja mineralne sirovine i geoloških struktura u rudniku Calamine, središnji Iran

Cilj je ovoga istraživanja identificirati mineralizirane zone unutar sedimentne strukture i njezine diskontinuitete poput granica slojeva i rasjeda. Za postizanje dubine istraživanja do 200 metara korišten je Loza-N model duboko prodirućega georadara (*Deep Ground Penetrating Radar* DGPR) s antenom od 25 MHz. Istraživanje je provedeno na etažama, etažnim ravninama i ravnome sjevernom platou rudnika Calamine Mehdiabad koji se nalazi u području Yazd u Iranu. Snimljena su ukupno 23 profila. Prikupljanje podataka za neke profile uključivalo je paralelne antene duž profila, dok se za druge koristio serijski pristup gdje su se antene odašiljača i prijamnika postupno pomicale duž istoga pravca po površini tla. Obrađeni radargrami odabranih profila uspoređeni su s podatcima iz bušotina prikupljenim duž istih profila. Geološka struktura uspješno je vizualizirana dvama različitim računalnim programima. Krot program učinkovito je razlikovao sve jedinice vapnenca i njihovu zonalnost. Kombinacijom GPR podataka s rezultatima bušotina bilo je moguće identificirati potencijalne zone rudnih minerala unutar jedinica lapora. Na temelju DGPR tragova na lokacijama bušotina visokokvalitetni rudni minerali u laporovitome vapnencu pokazali su pozitivne vrijednosti faze i amplitude predstavljene narančastim do crvenim nijansama na skali boja. Nasuprot tome, svijetlo zeleni i svijetlo sivi vapnenac koji sadržava željezni oksid i kalcitne vene pokazao je negativne vrijednosti faze i amplitude, a prikazan je zelenim do svijetlo plavim nijansama boje na skali. Tamnozeleni vapnenac pokazao je maksimalne negativne vrijednosti faze i amplitude, što se odražava u tamno plavim nijansama na skali. Konačno, svijetlo crveni vapnenac, koji vjerojatno sadržava niskokvalitetnu rudu, pokazao je pozitivne, ali minimalne vrijednosti faze i amplitude, vizualizirane žutim do narančastim nijansama boja.

Ključne riječi:
duboko prodirući georadar (DGPR), Loza-N DGPR sustav, geološka struktura, vapnenačke jedinice, rudnik Mehdiabad Calamine

Author's contribution

Nasrin **Sadrmohammadi (1)**)Master of Geology, Kharazmi University): DGPR interpretations and presentation of the results, investigation resources, provided the original draft, writing– review & editing. **Selma Kadioğlu (2)** (Academic/ Full Professor in Ankara University): DGPR interpretations and presentation of the results, review & editing. **Khalil Rezaei (3)** (Academic/ Associate Professor in Kharazmi University): data collection, review & editing. **Mahmoud Honarvar (4)** (Master of Geology): performed the field work, data collection.